Computationally Efficient Truncated Nuclear Norm Minimization for High Dynamic Range Imaging

Chul Lee, *Member, IEEE*, and Edmund Y. Lam, *Fellow, IEEE*

***Abstract*— Matrix completion is a rank minimization problem to recover a low-rank data matrix from a small subset of its entries. Since the matrix rank is nonconvex and discrete, many existing approaches approximate the matrix rank as the nuclear norm. However, the truncated nuclear norm is known to be a better approximation to the matrix rank than the nuclear norm, exploiting *a priori* target rank information about the problem in rank minimization. In this paper, we propose a computationally efficient truncated nuclear norm minimization algorithm for matrix completion, which we call TNNM-ALM. We reformulate the original optimization problem by introducing slack variables and considering noise in the observation. The central contribution of this paper is to solve it efficiently via the augmented Lagrange multiplier (ALM) method, where the optimization variables are updated by closed-form solutions. We apply the proposed TNNM-ALM algorithm to ghost-free high dynamic range imaging by exploiting the low-rank structure of irradiance maps from low dynamic range images. Experimental results on both synthetic and real visual data show that the proposed algorithm achieves significantly lower reconstruction errors and superior robustness against noise than the conventional approaches, while providing substantial improvement in speed, thereby applicable to a wide range of imaging applications.**

***Index Terms*— Matrix completion, rank minimization, nuclear norm minimization, augmented Lagrange multiplier method, high dynamic range imaging.**

I. Introduction

WE CONSIDER the problem of recovering an unknown matrix from a limited number of observed entries, which is well-known as the matrix completion problem [1]. This problem arises in a number of image processing applications, including object detection [2], denoising [3], image classification [4], [5], and high dynamic range (HDR) imaging [6]–[8], in which some entries of the data matrix may be corrupted or even missing in practice. For example, a set of pixels may be missing from an image due to transmission errors in the encoded bitstream or the deterioration of photographs. A common assumption in matrix completion is that the data have low intrinsic complexity, *i.e.*, the data matrix has (approximately) a low rank. Specifically, given the assumption of a low-rank data matrix $\mathbf{D} \in \mathbb{R}^{m \times n}$, the matrix completion problem, which estimates missing elements, can be formulated as

$$\begin{aligned} &\underset{\mathbf{X}}{\text{minimize}}\ \text{rank}(\mathbf{X}) \\ &\text{subject to}\ X_{ij} = D_{ij}, \quad \text{for}\ (i,j) \in \Omega, \end{aligned} \tag{1}$$

where $\mathbf{X} \in \mathbb{R}^{m \times n}$, and a sampled set of entries D_{ij} in set Ω is observed while other elements are missing.

However, since $\text{rank}(\mathbf{X})$ is a nonconvex and discrete function of $\mathbf{X}$, solving the optimization problem in (1) is intractable in practice. Therefore, previous approaches approximate the rank function to the nuclear norm of matrices [1], [9]–[11], *i.e.*, the sum of all singular values, which leads to a convex optimization problem. The nuclear norm has been shown to be the tightest convex lower bound of the rank function of matrices [10], and recent theoretical studies have shown that, under broad conditions, solving a convex optimization problem, *i.e.*, nuclear norm minimization subject to data constraints, can recover an unknown low-rank matrix from only a few observed entries [1], [10]–[13]. In addition, efficient algorithms for nuclear norm minimization for the low-rank matrix completion problem have been proposed [9], [11], [14]–[16].

While the previous nuclear norm minimization algorithms have strong theoretical guarantees [1], [9], [14], [17], they may fail to obtain the optimal solution in practical applications. This failure occurs because the nuclear norm-based algorithms minimize the sum of all singular values, while the matrix rank only corresponds to nonzero singular values. Moreover, the nuclear norm does not fully take into account *a priori* rank information about the problem in the optimization. For example, assuming that the scene is static, stacking irradiance maps from images of a scene captured with different exposure times, or equivalently different shutter speeds, forms a matrix of rank 1, and an HDR image can be obtained via rank minimization [8]. Another example is photometric stereo, which estimates surface shapes from multiple images taken under different lighting conditions. Under the Lambertian assumption, an image data matrix was shown to be rank 3 [18], and surface maps can be estimated by minimizing the matrix rank [19]. However, conventional nuclear norm minimization methods cannot exploit such given rank information, degrading the quality of results caused by outliers, such as occlusion by moving objects or saturated regions for HDR imaging and shadows or specularities for photometric stereo, respectively.

Manuscript received August 19, 2015; revised January 12, 2016 and May 22, 2016; accepted June 14, 2016. Date of publication June 24, 2016; date of current version July 14, 2016. This work was supported by the National Research Foundation of Korea (NRF) grant funded by the Korean Government (MSIP) under Grant NRF-2015R1A2A1A10076683 and under Grant NRF-2016R1C1B2010319. The associate editor coordinating the review of this manuscript and approving it for publication was Prof. Andrew Lumsdaine.

C. Lee is with the Department of Computer Engineering, Pukyong National University, Busan 48513, South Korea (e-mail: chullee@pknu.ac.kr).

E. Y. Lam is with the Department of Electrical and Electronic Engineering, The University of Hong Kong, Hong Kong (e-mail: elam@eee.hku.hk).

Color versions of one or more of the figures in this paper are available online at http://ieeexplore.ieee.org.

Digital Object Identifier 10.1109/TIP.2016.2585047

To address these limitations of the nuclear norm in matrix completion, a more accurate approximation to the matrix rank has recently been developed that achieves better control of the target rank of the low-rank solution, called the *truncated nuclear norm* [20]. The truncated nuclear norm is given by the sum of the smallest singular values. Since the original matrix has a low-rank structure, only a few largest singular values affect the approximation of the matrix rank, and thus the truncated nuclear norm leads to a better approximation to the matrix rank while producing the target rank.

While recent researches on low-rank matrix completion have focused on developing efficient nuclear norm minimization algorithms, it has been shown that the truncated nuclear norm can achieve better performance than the nuclear norm [20]. However, the main disadvantage of the truncated nuclear norm is its higher computational complexity in the optimization due to its two-step nature, and developing an efficient truncated nuclear norm minimization remains a significant open challenge.

In this work, to address the aforementioned open challenge, we propose a computationally efficient truncated nuclear norm minimization (TNNM) for matrix completion that is also robust against noise. Specifically, we make the following contributions:

- We develop a new algorithm for TNNM for matrix completion using the *augmented Lagrange multiplier (ALM)* method, which we call TNNM-ALM. We first reformulate the TNNM problem into a series of convex and non-convex subproblems. Then, we solve each of these subproblems efficiently using recent optimization techniques. In particular, we derive a rigorous closed-form solution to the convex subproblem, establishing the computational efficiency, which had previously been iteratively solved in the conventional method [20].
- We extend the TNNM-ALM algorithm for ghost-free HDR imaging to demonstrate its great potential in practical applications. Based on the assumption that the underlying background is static, we represent the background and moving objects as a low-rank matrix and a sparse matrix, respectively. Then, we formulate the background estimation as the low-rank matrix completion problem and solve it efficiently using TNNM-ALM.
- We experimentally show with both synthetic and real image datasets that TNNM-ALM can recover the low-rank matrix from noisy observations with significantly higher accuracy than the state-of-the-art approaches [16], [20]–[25], while providing substantial increases in speed. Furthermore, we show that TNNM-ALM can provide HDR images of comparable or even higher quality to those of competing algorithms [7], [8], [26], [27] with significantly reduced use of computational resources.

II. Related Work

A. Low-Rank Matrix Completion

As mentioned in the previous section, it is intractable in practice to directly solve the optimization problem in (1). Therefore, previous approaches use an approximate method via convex relaxation [1], [9]–[12]. Specifically, following notations in [9], let $\mathcal{P}_\Omega : \mathbb{R}^{m\times n} \rightarrow \mathbb{R}^{m\times n}$ denote the orthogonal projection of a matrix onto the subspace of matrices that have nonzero elements corresponding to the observed entries in Ω, *i.e.*,

$$[\mathcal{P}_\Omega(\mathbf{X})]_{ij} = \begin{cases} X_{ij}, & \text{if } (i,j) \in \Omega, \\ 0, & \text{otherwise.} \end{cases} \tag{2}$$

Then, the optimization problem in (1) can be reformulated approximating the rank function by the nuclear norm, *i.e.*,

$$\begin{aligned} &\underset{\mathbf{X}}{\text{minimize}} \ \|\mathbf{X}\|_* \\ &\text{subject to } \mathcal{P}_\Omega(\mathbf{X}) = \mathcal{P}_\Omega(\mathbf{D}), \end{aligned} \tag{3}$$

where $\|\mathbf{X}\|_* = \sum_{k=1}^{\min(m,n)} \sigma_k(\mathbf{X})$ is the nuclear norm, and $\sigma_k(\mathbf{X})$ denotes the kth largest singular value of $\mathbf{X}$.

Several algorithms have been proposed to solve the optimization problem in (3). In [28], Fazel reformulated (3) as a semi-definite programming (SDP) problem and solved it using the interior-point method, but its applicability is limited in practice due to its significant computational complexity. Cai *et al.* [9] further approximated the problem for a strong convex objective function, and then developed the singular value thresholding (SVT) algorithm. The optimization in (3) was reformulated as the nuclear norm regularized least squares problem, and Ma *et al.* [11] applied the fixed point and Bregman iterative method to solve it. In addition, the accelerated proximal gradient (APG) algorithm [14], [29] and the SOFT-IMPUTE algorithm [15] have been developed to efficiently solve the reformulated problem. While these algorithms not only solve the nuclear norm minimization problem efficiently but also give a theoretical guarantee, they may fail to obtain the optimal solutions in practice. Specifically, as mentioned in Section I, the rank may not be well approximated by the nuclear norm. Moreover, the nuclear norm cannot exploit *a priori* target rank information about a specific problem.

Matrix factorization-based matrix completion has been attempted that can exploit *a priori* rank information [21], [22], [30]. For example, in [22], Wen *et al.* solved the following low-rank matrix factorization problem

$$\begin{aligned} &\underset{\mathbf{U},\mathbf{V},\mathbf{Z}}{\text{minimize}} \ \frac{1}{2}\|\mathbf{UV} - \mathbf{Z}\|_F^2 \\ &\text{subject to } \mathcal{P}_\Omega(\mathbf{Z}) = \mathcal{P}_\Omega(\mathbf{D}), \end{aligned} \tag{4}$$

where $\mathbf{Z} \in \mathbb{R}^{m\times n}$, $\mathbf{U} \in \mathbb{R}^{m\times r}$ and $\mathbf{V} \in \mathbb{R}^{r\times n}$ for a given rank r, and $\|\mathbf{X}\|_F = \left(\sum_{ij} |X_{ij}|^2\right)^{1/2}$ denotes the Frobenius norm of a matrix. It is known that, while the matrix factorization problem in (4) can generally be solved faster than the nuclear norm minimization-based approaches, one may fail to obtain a global solution due to the nonconvexity [22].

To address the aforementioned limitations of the nuclear norm in rank minimization, better approximations to the matrix rank have been proposed. These algorithms attempt to minimize the sum of the least $(\min(m,n)-r)$ singular values based on the observation that the rank of a matrix only corresponds to the first r nonzero singular values. This technique is called truncated nuclear norm regularization (TNNR) [20] or partial sum minimization of singular values (PSSV) [23], [25].

More specifically, following notations in [20], given the target rank r, the optimization in (3) can be rewritten as

$$\begin{aligned} &\underset{\mathbf{X}}{\text{minimize}} \ \|\mathbf{X}\|_r \\ &\text{subject to } \mathcal{P}_\Omega(\mathbf{X}) = \mathcal{P}_\Omega(\mathbf{D}), \end{aligned} \tag{5}$$

where $\|\mathbf{X}\|_r = \sum_{k=r+1}^{\min(m,n)} \sigma_k(\mathbf{X})$ is the truncated nuclear norm. The PSSV [23] solves a problem similar to that in (5) for the robust principal component analysis (RPCA) [31], but it can be regarded as a case when all elements in data matrix $\mathbf{D}$ are observed. In [25], it was shown that PSSV can be extended to solve the problem in (5), but detailed theoretical analysis has not been provided. Moreover, if only partial data are observed, PSSV requires higher computational complexity to solve RPCA [8]. Recently, more generalized nuclear norms have been studied [24], [32], [33]. Although the truncated nuclear norm is a special case of solving such generalized forms, the truncated nuclear norm suggests how we can encourage the rank constraint.

Note, however, that $\|\mathbf{X}\|_r$ in (5) is nonconvex. Therefore, to solve the problem, Hu *et al.* [20] reformulated the problem as follows:

$$\begin{aligned} &\underset{\mathbf{X}}{\text{minimize}} \ \|\mathbf{X}\|_* - \underset{\mathbf{A}\mathbf{A}^T=\mathbf{I},\, \mathbf{B}\mathbf{B}^T=\mathbf{I}}{\text{maximize}} \operatorname{tr}(\mathbf{A}\mathbf{X}\mathbf{B}^T) \\ &\text{subject to } \mathcal{P}_\Omega(\mathbf{X}) = \mathcal{P}_\Omega(\mathbf{D}), \end{aligned} \tag{6}$$

where $\mathbf{A} \in \mathbb{R}^{r\times m}$ and $\mathbf{B} \in \mathbb{R}^{r\times n}$. The optimization in (6) can be solved alternatively by separating it into two steps. Specifically, at each iteration, given an estimate of $\mathbf{X}$, both $\mathbf{A}$ and $\mathbf{B}$ are computed. Then, an estimate of $\mathbf{X}$ is updated with $\mathbf{A}$ and $\mathbf{B}$ fixed. Since we need to solve two sets of optimizations alternatively, a nested loop requiring high computational complexity is needed to solve (6).

B. Ghost-Free HDR Imaging

The goal of ghost-free HDR imaging is to obtain high-quality HDR images in the presence of camera or object motions in input images. Due to its practical importance, a lot of researches have been made for undertaking this challenge [34], and each of these algorithms approaches from a different perspective. In this section, however, we only focus our review on algorithms that are closely related to the proposed HDR imaging. For a more detailed survey on ghost-free HDR imaging, we refer the readers to [34].

One approach to ghost-free HDR imaging is to register low dynamic range (LDR) images before HDR image synthesis using correspondence estimation. For example, in [27], [35], and [36], a patch-based matching strategy was employed to recover or reconstruct the potential ghost regions in the output image by finding information from a subset of input images. While these algorithms provide high-quality HDR images, the main disadvantage is its high computational complexity due to the intensive searching.

Another approach is to alleviate the contributions of regions on moving objects detected by ghost region detection. For example, Gallo *et al.* [37] used the deviation from linearity to measure ghost effects, assuming that the background irradiance is linear with respect to exposure times. Heo *et al.* [26] detected ghost regions employing the joint probability density between different exposure images and then further refined these regions using energy minimization.

Recently, to better exploit the linearity of irradiances, a rank minimization framework has been employed in ghost-free HDR imaging [7], [8], [38]. Oh *et al.* [8] attempted to align input images and detect moving objects simultaneously using a rank minimization approach to compensate for camera motion. Further, they extended their work employing low-rank matrix completion [1]. Lee *et al.* [7] developed low-rank matrix completion-based HDR imaging with multiple physical constraints on the properties of ghost regions. Bhardwaj and Raman [38] extended the ALM-based rank minimization algorithm [16] to improve HDR image quality. However, while recent researches on rank minimization-based HDR imaging approaches provide high-quality results, such sophisticated algorithms require significant computational resources.

III. Proposed Algorithm (TNNM-ALM)

A. Problem Formulation

We consider a generalization of (5) for real-world data acquisition scenarios. Specifically, only a set of entries that are corrupted by a small amount of noise is observed in practice [13], *i.e.*, $\mathcal{P}_\Omega(\mathbf{X}+\mathbf{N}) = \mathcal{P}_\Omega(\mathbf{D})$, where $\mathbf{N}$ is a noise matrix. The noise level is given by $\|\mathcal{P}_\Omega(\mathbf{N})\|_F \le \delta$ for some $\delta \ge 0$. Then, introducing slack variables as similarly done in [39], we reformulate the TNNM problem in (5) as

$$\begin{aligned} &\underset{\mathbf{X},\,\mathbf{S}}{\text{minimize}} \ \|\mathbf{X}\|_r \\ &\text{subject to } \mathbf{X}+\mathbf{S} = \mathcal{P}_\Omega(\mathbf{D}), \\ &\qquad\qquad \|\mathcal{P}_\Omega(\mathbf{S})\|_F \le \delta, \end{aligned} \tag{7}$$

where $\mathbf{S} \in \mathbb{R}^{m\times n}$ is a matrix of slack variables to compensate for the unknown entries in $\mathbf{D}$. Although the introduction of slack variables $\mathbf{S}$ in (7) increases the number of optimization variables, it enables us to obtain a closed-form solution of $\mathbf{X}$ at each iteration during the optimization as will be shown in Section III-B, which is otherwise intractable due to the sampling operator $\mathcal{P}_\Omega$. Moreover, the slack variables enable us to solve the matrix completion problem with sparse errors, as will be shown in Section IV.

The inexact ALM approach for matrix completion (IALM-MC) [16] also employs slack variables in its formulation. However, the main novelties we make in the reformulation in (7) over IALM-MC are as follows: First, we minimize the truncated nuclear norm to fully exploit the target rank information, while IALM-MC minimizes the nuclear norm. Second, the solution $\mathbf{S}_{k+1}$ at each iteration of the optimization is derived more rigorously as will be shown in Section III-B, whereas it is chosen heuristically in [16], although it guarantees that the constraints hold. Third, we consider noise components in the observed data for more realistic scenarios.

B. Solution to the Optimization

We first introduce the partial singular value thresholding (PSVT) operator [23], which will be used at each iteration of the proposed TNNM-ALM. Specifically, a matrix $\mathbf{A} \in \mathbb{R}^{m\times n}$ can be decomposed as the sum of two matrices via

the singular value decomposition (SVD), *i.e.*, $\mathbf{A} = \mathbf{U}\mathbf{\Sigma}_1\mathbf{V}^T + \mathbf{U}\mathbf{\Sigma}_2\mathbf{V}^T$, where $\mathbf{\Sigma}_1 = \text{diag}(\sigma_1, \cdots, \sigma_r, 0, \cdots, 0)$ and $\mathbf{\Sigma}_2 = \text{diag}(0, \cdots, 0, \sigma_{r+1}, \cdots, \sigma_{\min(m,n)})$, respectively. Then, for $\tau, r > 0$, a globally optimal solution to the following problem

$$\underset{\mathbf{B}}{\text{minimize}}\ \tau\|\mathbf{B}\|_r + \frac{1}{2}\|\mathbf{B} - \mathbf{A}\|_F^2 \tag{8}$$

is given by the PSVT operator, defined as

$$\mathbb{P}_{r,\tau}(\mathbf{A}) = \mathbf{U}(\mathbf{\Sigma}_1 + \mathcal{S}_\tau(\mathbf{\Sigma}_2))\mathbf{V}^T, \tag{9}$$

where $\mathcal{S}_\tau(\mathbf{A})$ denotes the entry-wise soft-thresholding operator [40], *i.e.*, $[\mathcal{S}_\tau(\mathbf{A})]_{ij} = \text{sign}(A_{ij}) \cdot \max\{|A_{ij}| - \tau, 0\}$. Note that the PSVT operator in (9) is a special case of solving the weighted nuclear norm-based objective function [32], [33]. Therefore, the proposed TNNM-ALM, which uses PSVT to solve a subproblem, can also be used for more general weighted nuclear norm minimization problems.

The following theorem establishes the computational efficiency of TNNM-ALM over conventional methods, as it is used at each iteration to obtain the closed-form solution to the subproblem.

Theorem 1: For $\mathbf{B} \in \mathbb{R}^{m\times n}$ and $\delta \geq 0$, the optimal solution to the following optimization problem

$$\begin{aligned} &\underset{\mathbf{A}}{\text{minimize}}\ \|\mathbf{A} - \mathbf{B}\|_F^2 \\ &\text{subject to}\ \|\mathcal{P}_\Omega(\mathbf{A})\|_F \leq \delta, \end{aligned} \tag{10}$$

is given by

$$\widehat{\mathbf{A}} = \mathcal{P}_{\Omega^c}(\mathbf{B}) + \min\left\{\frac{\delta}{\|\mathcal{P}_\Omega(\mathbf{B})\|_F}, 1\right\}\mathcal{P}_\Omega(\mathbf{B}). \tag{11}$$

Proof: When $(i, j) \notin \Omega$, it is obvious that the solution to (10) is given by $\widehat{A}_{ij} = B_{ij}$, or equivalently $\mathcal{P}_{\Omega^c}(\widehat{\mathbf{A}}) = \mathcal{P}_{\Omega^c}(\mathbf{B})$. Thus, we focus on the case $(i, j) \in \Omega$. Let us denote $\mathbf{Z} = \mathcal{P}_\Omega(\mathbf{A})$ and $\mathbf{W} = \mathcal{P}_\Omega(\mathbf{B})$ for simpler notations, then the optimization in (10) can be rewritten as

$$\begin{aligned} &\underset{\mathbf{Z}}{\text{minimize}}\ \|\mathbf{Z} - \mathbf{W}\|_F^2 \\ &\text{subject to}\ \|\mathbf{Z}\|_F^2 \leq \delta^2. \end{aligned} \tag{12}$$

We define the Lagrangian function as

$$\mathcal{L}(\mathbf{Z}, \lambda) = \|\mathbf{Z} - \mathbf{W}\|_F^2 + \lambda\big(\|\mathbf{Z}\|_F^2 - \delta^2\big), \tag{13}$$

where λ is the Lagrange multiplier. The Karush-Kuhn-Tucker (KKT) conditions are [41]

$$\|\mathbf{Z}\|_F - \delta \leq 0, \tag{14}$$

$$\lambda \geq 0, \tag{15}$$

$$\lambda(\|\mathbf{Z}\|_F - \delta) = 0, \tag{16}$$

$$(1 + \lambda)\mathbf{Z} - \mathbf{W} = \mathbf{0}, \tag{17}$$

where $\mathbf{0}$ denotes the matrix with all zero elements. In the derivation of (17), we use the derivative of the Frobenius norm of a matrix $\frac{\partial}{\partial \mathbf{X}}\|\mathbf{X}\|_F^2 = \frac{\partial}{\partial \mathbf{X}}\text{tr}(\mathbf{X}\mathbf{X}^T) = 2\mathbf{X}$.

Substituting $\mathbf{Z}$ from (17) into (16) yields

$$\lambda(\|\mathbf{Z}\|_F - \delta) = \frac{\lambda}{1 + \lambda}\big[\|\mathbf{W}\|_F - (1 + \lambda)\delta\big] = 0. \tag{18}$$

We consider two cases: $\|\mathbf{W}\|_F < \delta$ and $\|\mathbf{W}\|_F \geq \delta$. In the former, from (15), $\|\mathbf{W}\|_F - (1+\lambda)\delta < 0$, which leads to $\lambda = 0$. Therefore, we have $\mathbf{Z} = \mathbf{W}$. In the latter, $\|\mathbf{W}\|_F - (1+\lambda)\delta = 0$. Then, by substituting $(1+\lambda)$ into (17), we have $\mathbf{Z} = \frac{\delta}{\|\mathbf{W}\|_F}\mathbf{W}$. Combining the two cases yields

$$\mathcal{P}_\Omega(\widehat{\mathbf{A}}) = \min\left\{\frac{\delta}{\|\mathcal{P}_\Omega(\mathbf{B})\|_F}, 1\right\}\mathcal{P}_\Omega(\mathbf{B}). \tag{19}$$

Since $\widehat{\mathbf{A}} = \mathcal{P}_{\Omega^c}(\widehat{\mathbf{A}}) + \mathcal{P}_\Omega(\widehat{\mathbf{A}})$, we obtain (11). ■

We now derive the solution to the optimization problem in (7). Recent advances in rank minimization have shown that the high-dimensional nuclear norm minimization can be efficiently solved [14], [16], [42]. In particular, Lin *et al.* [16] adopted the ALM method [43], [44] to solve the nuclear norm minimization problem, which is known to be efficient due to its fast convergence and scalability. Here, we show how we adopt the ALM method to efficiently solve the TNNM problem in (7).

The ALM method solves a series of unconstrained subproblems instead of the original constrained optimization problem. Specifically, for our problem in (7), we first define the augmented Lagrangian function $\mathcal{L}(\mathbf{X}, \mathbf{S}, \mathbf{\Lambda}, \mu)$ as

$$\begin{aligned} \mathcal{L}(\mathbf{X}, \mathbf{S}, \mathbf{\Lambda}, \mu) = \|\mathbf{X}\|_r + \langle \mathbf{\Lambda}, \mathcal{P}_\Omega(\mathbf{D}) - \mathbf{X} - \mathbf{S}\rangle \\ + \frac{\mu}{2}\|\mathcal{P}_\Omega(\mathbf{D}) - \mathbf{X} - \mathbf{S}\|_F^2, \end{aligned} \tag{20}$$

where $\mu > 0$ is a parameter to penalize the linear equality constraint, $\langle \mathbf{A}, \mathbf{B}\rangle = \text{tr}(\mathbf{A}\mathbf{B}^T)$ denotes the matrix inner product, and $\mathbf{\Lambda} \in \mathbb{R}^{m\times n}$ is a Lagrange multiplier matrix. It is known that a solution to the original optimization problem given in (7) can be obtained by minimizing its augmented Lagrangian $\mathcal{L}(\mathbf{X}, \mathbf{S}, \mathbf{\Lambda}, \mu)$ for an estimate of $\mathbf{\Lambda}$ and a sufficiently large value of μ [44]. The ALM algorithm iteratively estimates both the optimal solution and the Lagrange multiplier until convergence, *i.e.*,

$$(\mathbf{X}_{k+1}, \mathbf{S}_{k+1}) = \underset{\mathbf{X}, \mathbf{S}}{\arg\min}\ \mathcal{L}(\mathbf{X}, \mathbf{S}, \mathbf{\Lambda}_k, \mu_k), \tag{21}$$

$$\mathbf{\Lambda}_{k+1} = \mathbf{\Lambda}_k + \mu_k(\mathcal{P}_\Omega(\mathbf{D}) - \mathbf{X}_{k+1} - \mathbf{S}_{k+1}), \tag{22}$$

where k is the iteration index.

Joint optimization over both $\mathbf{X}$ and $\mathbf{S}$ in (21) is intractable in practice. A common strategy to solve this joint optimization is to employ the alternating direction method of multipliers (ADMM) [45], which separates the optimization over each variable while fixing the other one. Specifically, we iteratively update $\mathbf{X}$ and $\mathbf{S}$ in (21) one by one, and then $\mathbf{\Lambda}$ in (22). Although the subproblems involve solving convex and nonconvex optimization problems, respectively, each can be solved efficiently by a closed-form solution, which can reduce the computational complexity significantly compared with [20]. These subproblems are described below.

Updating X. In the first step, given estimates of $\mathbf{S}_k$ and $\mathbf{\Lambda}_k$, we update $\mathbf{X}$ as

$$\begin{aligned} \mathbf{X}_{k+1} &= \underset{\mathbf{X}}{\arg\min}\ \mathcal{L}(\mathbf{X}, \mathbf{S}_k, \mathbf{\Lambda}_k, \mu_k) \\ &= \underset{\mathbf{X}}{\arg\min}\ \|\mathbf{X}\|_r + \langle \mathbf{\Lambda}_k, \mathcal{P}_\Omega(\mathbf{D}) - \mathbf{X} - \mathbf{S}_k\rangle \\ &\quad + \frac{\mu_k}{2}\|\mathcal{P}_\Omega(\mathbf{D}) - \mathbf{X} - \mathbf{S}_k\|_F^2 \\ &= \underset{\mathbf{X}}{\arg\min}\ \|\mathbf{X}\|_r + \frac{\mu_k}{2}\|\mathbf{X} - \mathcal{P}_\Omega(\mathbf{D}) + \mathbf{S}_k - \mu_k^{-1}\mathbf{\Lambda}_k\|_F^2. \end{aligned} \tag{23}$$

The closed-form solution to the problem in (23) can be obtained by the PSVT operator in (9) as

$$\mathbf{X}_{k+1} = \mathbb{P}_{r,\mu_k^{-1}}\left(\mathcal{P}_{\Omega}(\mathbf{D}) - \mathbf{S}_k + \mu_k^{-1}\mathbf{\Lambda}_k\right). \tag{24}$$

Updating S. Next, we estimate $\mathbf{S}$, given $\mathbf{\Lambda}_k$ and $\mathbf{X}_{k+1}$ in (24). Specifically, the optimization in (21) can be rewritten as

$$\begin{aligned}\mathbf{S}_{k+1} &= \underset{\|\mathcal{P}_{\Omega}(\mathbf{S})\|_F \le \delta}{\arg\min}\ \mathcal{L}(\mathbf{X}_{k+1}, \mathbf{S}, \mathbf{\Lambda}_k, \mu_k) \\ &= \underset{\|\mathcal{P}_{\Omega}(\mathbf{S})\|_F \le \delta}{\arg\min}\ \langle \mathbf{\Lambda}_k, \mathcal{P}_{\Omega}(\mathbf{D}) - \mathbf{X}_{k+1} - \mathbf{S}\rangle \\ &\quad + \frac{\mu_k}{2}\|\mathcal{P}_{\Omega}(\mathbf{D}) - \mathbf{X}_{k+1} - \mathbf{S}\|_F^2 \\ &= \underset{\|\mathcal{P}_{\Omega}(\mathbf{S})\|_F \le \delta}{\arg\min}\ \frac{\mu_k}{2}\|\mathbf{S} - \mathcal{P}_{\Omega}(\mathbf{D}) + \mathbf{X}_{k+1} - \mu_k^{-1}\mathbf{\Lambda}_k\|_F^2 \\ &= \underset{\|\mathcal{P}_{\Omega}(\mathbf{S})\|_F \le \delta}{\arg\min}\ \|\mathbf{S} - \mathbf{Y}_{k+1}\|_F^2, \end{aligned} \tag{25}$$

where we denote $\mathbf{Y}_{k+1} = \mathcal{P}_{\Omega}(\mathbf{D}) - \mathbf{X}_{k+1} + \mu_k^{-1}\mathbf{\Lambda}_k$ for simpler notations. Then, according to Theorem 1, we can obtain the closed-form solution to the subproblem in (25), given by

$$\mathbf{S}_{k+1} = \mathcal{P}_{\Omega^c}(\mathbf{Y}_{k+1}) + \min\left\{\frac{\delta}{\|\mathcal{P}_{\Omega}(\mathbf{Y}_{k+1})\|_F}, 1\right\}\mathcal{P}_{\Omega}(\mathbf{Y}_{k+1}). \tag{26}$$

Updating Λ. Finally, given $\mathbf{X}_{k+1}$ and $\mathbf{S}_{k+1}$, the Lagrange multiplier matrix $\mathbf{\Lambda}$ is updated following the strategy of the ALM method [16], [43], [44], *i.e.*,

$$\mathbf{\Lambda}_{k+1} = \mathbf{\Lambda}_k + \mu_k(\mathcal{P}_{\Omega}(\mathbf{D}) - \mathbf{X}_{k+1} - \mathbf{S}_{k+1}). \tag{27}$$

Here, notice that all the optimization variables $\mathbf{X}$, $\mathbf{S}$, and $\mathbf{\Lambda}$ are updated in a single step via the closed-form solutions in (24), (26), and (27), respectively, allowing the optimization problem to be efficiently solved. This computational efficiency is a major advantage of the proposed TNNM-ALM over the conventional algorithm [20], as will be discussed in Section V.

Finally, we update the penalty parameter μ by employing an adaptive update strategy [46] as

$$\mu_{k+1} = \begin{cases} \min\{\rho\mu_k, \mu_{\max}\}, & \text{if } \dfrac{\mu_k\|\mathbf{X}_{k+1} - \mathbf{X}_k\|_F}{\|\mathcal{P}_{\Omega}(\mathbf{D})\|_F} < \kappa, \\ \mu_k, & \text{otherwise,} \end{cases} \tag{28}$$

where $\mu_{\max}$ denotes an upper bound of $\{\mu_k\}$, and $\rho > 1$ and $\kappa > 0$ are user parameters chosen in advance.

The optimization variables $\mathbf{X}$, $\mathbf{S}$, $\mathbf{\Lambda}$, and μ are iteratively updated until convergence. We define the convergence rate at the kth iteration as

$$\xi_k = \frac{\max\{\|\mathcal{P}_{\Omega}(\mathbf{D}) - \mathbf{X}_k - \mathbf{S}_k\|_F, \|\mathbf{X}_k - \mathbf{X}_{k-1}\|_F\}}{\|\mathcal{P}_{\Omega}(\mathbf{D})\|_F}, \tag{29}$$

and run the iteration until $\xi_k < 10^{-4}$. The complete algorithm to solve the optimization in (7) is summarized in Algorithm 1. Note that, while the convergence analysis for the ALM method alternating convex optimization problems has been studied [16], [39], one for alternating between the nonconvex and convex optimization problems given in (23) and (25), respectively, has not been theoretically established.

Algorithm 1 TNNM-ALM: Optimization for Solving (7) via the ALM Method

Input: $\mathbf{D} \in \mathbb{R}^{m\times n}$, Ω, r, δ, κ.

1: Initialize $\mathbf{X}_1 = \mathbf{D}$, $\mathbf{\Lambda}_1 = \mathbf{D}$, $\mu_1 > 0$, $\rho > 1$, and $k = 1$.
2: **while** not converged **do**
3: $\quad\mathbf{X}_{k+1} = \mathbb{P}_{r,\mu_k^{-1}}\left(\mathcal{P}_{\Omega}(\mathbf{D}) - \mathbf{S}_k + \mu_k^{-1}\mathbf{\Lambda}_k\right)$.
4: $\quad\mathbf{S}_{k+1} = \mathcal{P}_{\Omega^c}(\mathbf{Y}_{k+1}) + \min\left\{\frac{\delta}{\|\mathcal{P}_{\Omega}(\mathbf{Y}_{k+1})\|_F}, 1\right\}\mathcal{P}_{\Omega}(\mathbf{Y}_{k+1})$, where $\mathbf{Y}_{k+1} = \mathcal{P}_{\Omega}(\mathbf{D}) - \mathbf{X}_{k+1} + \mu_k^{-1}\mathbf{\Lambda}_k$.
5: $\quad\mathbf{\Lambda}_{k+1} = \mathbf{\Lambda}_k + \mu_k(\mathcal{P}_{\Omega}(\mathbf{D}) - \mathbf{X}_{k+1} - \mathbf{S}_{k+1})$.
6: $\quad\mu_{k+1} = \begin{cases}\min\{\rho\mu_k, \mu_{\max}\}, & \text{if } \frac{\mu_k\|\mathbf{X}_{k+1} - \mathbf{X}_k\|_F}{\|\mathcal{P}_{\Omega}(\mathbf{D})\|_F} < \kappa, \\ \mu_k, & \text{otherwise.}\end{cases}$
7: $\quad k = k + 1$.
8: **end while**

Output: $\widehat{\mathbf{X}} = \mathbf{X}_k$

However, extensive experiments have shown that it converges well in practice [8], [23], [25]. We will also show experimentally in Section V that the proposed TNNM-ALM converges well with higher accuracy and faster than conventional algorithm [20].

Note that, since the proposed TNNM-ALM uses the PSVT operator in (24), it inherits the same limitation from PSSV [23], [25]. Specifically, when the span of the observed entries is less than the target rank due to a very limited number of samples, TNNM-ALM fails to satisfy the rank constraint and produces a rank lower than the target rank. However, as the results in Section V-A will show, the proposed TNNM-ALM achieves superior reconstruction performance than PSSV even when a small number of samples is observed.

IV. HDR Image Synthesis via TNNM-ALM

We apply the proposed TNNM-ALM algorithm to ghost-free HDR image synthesis. The input is a set of LDR images taken with different exposure times, and the goal is to composite a high-quality HDR image while alleviating the contributions of regions on moving objects in the input images. Recent researches [6]–[8] have shown that the rank minimization framework can be applied to HDR imaging to produce high-quality images. In particular, the work in [8] focuses on the application of the rank minimization framework described in [23] and [25] to HDR imaging. Here, we show that the application of TNNM-ALM to HDR imaging provides comparable or even better results to those of the state-of-the-art methods, while requiring significantly less computational resources. In this work, we assume that all input images are aligned by using a static camera or using pre-registration techniques [34]. However, note that batch image alignment can also be easily incorporated into the rank minimization framework [8], [47]. We omit such a modification for clarity, since our main goal in this work is to show how TNNM-ALM can be applied to HDR imaging.

A. Problem Formulation

We are given a set of images taken with different exposure times $\{\text{vec}(Z_1), \text{vec}(Z_2), \ldots, \text{vec}(Z_n)\}$, where

$\text{vec}(Z_i) \in \mathbb{R}^{m\times 1}$ denotes a vector of pixel values, and m and n are the number of pixels in an image and the number of input images, respectively. Then, using the camera response function [48], we construct the observed irradiance matrix $\mathbf{D} = \{\text{vec}(I_1), \text{vec}(I_2), \ldots, \text{vec}(I_n)\}$, where $\text{vec}(I_i)$ is the irradiance vector for the ith image.

The scene irradiance can be decomposed into the underlying background and moving objects. Specifically, the irradiance matrix $\mathbf{D}$ can be represented as the sum of two matrices $\mathbf{X}$ and $\mathbf{E}$, which correspond to the underlying background scene and moving objects, respectively. Since each column of matrix $\mathbf{X}$, corresponding to each input image, is spanned by the sensor irradiance vector of a static scene, matrix $\mathbf{X}$ has low rank, and $\mathbf{E}$ is a sparse matrix, *i.e.*, most elements in $\mathbf{E}$ are zero. In addition, we assume that only a limited number of observations can be made in HDR imaging in general due to under- and over-exposed regions in input images. However, note that we can also select preferable objects or regions that will appear in the synthesized HDR image by masking images [8]. Irradiance estimation for ghost-free HDR imaging can then be formulated as the following rank minimization problem

$$\begin{aligned} &\underset{\mathbf{X},\mathbf{E}}{\text{minimize}}\ \text{rank}(\mathbf{X}) + \lambda\|\mathbf{E}\|_0 \\ &\text{subject to}\ \mathcal{P}_\Omega(\mathbf{X}+\mathbf{E}) = \mathcal{P}_\Omega(\mathbf{D}). \end{aligned} \tag{30}$$

To solve the optimization problem in (30), we approximate the rank function and the ℓ_0-norm $\|\mathbf{E}\|_0$ by the truncated nuclear norm $\|\mathbf{X}\|_r$ and the ℓ_1-norm $\|\mathbf{E}\|_1$, respectively. Then, given the target rank r, the optimization in (30) can be rewritten as

$$\begin{aligned} &\underset{\mathbf{X},\mathbf{E}}{\text{minimize}}\ \|\mathbf{X}\|_r + \lambda\|\mathbf{E}\|_1 \\ &\text{subject to}\ \mathcal{P}_\Omega(\mathbf{X}+\mathbf{E}) = \mathcal{P}_\Omega(\mathbf{D}), \end{aligned} \tag{31}$$

where λ controls the relative importance between the rank of $\mathbf{X}$ and the sparsity of $\mathbf{E}$. Assuming that the underlying scene is static, we set the target rank to $r = 1$.

B. Optimization

As similarly done in Section III, we develop a computationally efficient algorithm to solve the optimization problem in (31). Oh *et al.* [8] also solved the optimization in (31) using the ALM method. However, because of the sampling operator $\mathcal{P}_\Omega$, they could not update the optimization variable in a closed-form manner, and instead solved it iteratively, which requires higher computational resources. The main novelty of the proposed algorithm over [8] is that we update the optimization variables by closed-form solutions, enabling it to be more efficient than the conventional algorithm [8]. We rewrite the problem in (31), introducing slack variables, as

$$\begin{aligned} &\underset{\mathbf{X},\mathbf{E},\mathbf{S}}{\text{minimize}}\ \|\mathbf{X}\|_r + \lambda\|\mathbf{E}\|_1 \\ &\text{subject to}\ \mathbf{X}+\mathbf{E}+\mathbf{S} = \mathcal{P}_\Omega(\mathbf{D}), \\ &\qquad\qquad \|\mathcal{P}_\Omega(\mathbf{S})\|_F \le \delta. \end{aligned} \tag{32}$$

We define the augmented Lagrangian function for (32), given by

$$\begin{aligned} \mathcal{L}(\mathbf{X},\mathbf{E},\mathbf{S},\mathbf{\Lambda},\mu) = {} & \|\mathbf{X}\|_r + \lambda\|\mathbf{E}\|_1 \\ & + \langle \mathbf{\Lambda}, \mathcal{P}_\Omega(\mathbf{D}) - \mathbf{X} - \mathbf{E} - \mathbf{S}\rangle \\ & + \frac{\mu}{2}\|\mathcal{P}_\Omega(\mathbf{D}) - \mathbf{X} - \mathbf{E} - \mathbf{S}\|_F^2. \end{aligned} \tag{33}$$

We find the stationary point of the augmented Lagrangian function by splitting the problem into subproblems, solving the sequence of subproblems

$$\mathbf{X}_{k+1} = \underset{\mathbf{X}}{\arg\min}\ \mathcal{L}(\mathbf{X},\mathbf{E}_k,\mathbf{S}_k,\mathbf{\Lambda}_k,\mu_k), \tag{34}$$

$$\mathbf{E}_{k+1} = \underset{\mathbf{E}}{\arg\min}\ \mathcal{L}(\mathbf{X}_{k+1},\mathbf{E},\mathbf{S}_k,\mathbf{\Lambda}_k,\mu_k), \tag{35}$$

$$\mathbf{S}_{k+1} = \underset{\|\mathcal{P}_\Omega(\mathbf{S})\|_F\le\delta}{\arg\min}\ \mathcal{L}(\mathbf{X}_{k+1},\mathbf{E}_{k+1},\mathbf{S},\mathbf{\Lambda}_k,\mu_k), \tag{36}$$

and updating the Lagrange multiplier by

$$\mathbf{\Lambda}_{k+1} = \mathbf{\Lambda}_k + \mu_k(\mathcal{P}_\Omega(\mathbf{D}) - \mathbf{X}_{k+1} - \mathbf{E}_{k+1} - \mathbf{S}_{k+1}). \tag{37}$$

We now describe how each subproblem is solved.

Subproblems. According to the PSVT operator in (9) and Theorem 1, the closed-form solutions to the subproblems in (34) and (36) are, respectively, given by

$$\mathbf{X}_{k+1} = \mathbb{P}_{r,\mu_k^{-1}}\Big(\mathcal{P}_\Omega(\mathbf{D}) - \mathbf{E}_k - \mathbf{S}_k + \mu_k^{-1}\mathbf{\Lambda}_k\Big), \tag{38}$$

$$\mathbf{S}_{k+1} = \mathcal{P}_{\Omega^c}(\mathbf{Y}_{k+1}) + \min\left\{\frac{\delta}{\|\mathcal{P}_\Omega(\mathbf{Y}_{k+1})\|_F}, 1\right\}\mathcal{P}_\Omega(\mathbf{Y}_{k+1}), \tag{39}$$

where $\mathbf{Y}_{k+1} = \mathcal{P}_\Omega(\mathbf{D}) - \mathbf{X}_{k+1} - \mathbf{E}_{k+1} + \mu_k^{-1}\mathbf{\Lambda}_k$.

The main difference between solving the optimization problems in (20) and (33) is on updating $\mathbf{E}$, and thus solving the optimization in (33) for $\mathbf{E}$ is the main contribution of this section. Here, given $\mathbf{X}_{k+1}$, $\mathbf{S}_k$, and $\mathbf{\Lambda}_k$, we solve the following optimization problem:

$$\begin{aligned} \mathbf{E}_{k+1} &= \underset{\mathbf{E}}{\arg\min}\ \lambda\|\mathbf{E}\|_1 + \langle \mathbf{\Lambda}_k, \mathcal{P}_\Omega(\mathbf{D}) - \mathbf{X}_{k+1} - \mathbf{E} - \mathbf{S}_k\rangle \\ &\quad + \frac{\mu_k}{2}\|\mathcal{P}_\Omega(\mathbf{D}) - \mathbf{X}_{k+1} - \mathbf{E} - \mathbf{S}_k\|_F^2 \\ &= \underset{\mathbf{E}}{\arg\min}\ \lambda\|\mathbf{E}\|_1 \\ &\quad + \frac{\mu_k}{2}\|\mathbf{E} - \mathcal{P}_\Omega(\mathbf{D}) - \mathbf{X}_{k+1} - \mathbf{S}_k + \mu_k^{-1}\mathbf{\Lambda}_k\|_F^2. \end{aligned} \tag{40}$$

The objective function in (40), which consists of the proximity term and the ℓ_1-norm term, can be effectively minimized by the element-wise soft-thresholding operator $\mathcal{S}_\tau(\cdot)$ [40]. Thus, the closed-form solution to (40) can be obtained by

$$\mathbf{E}_{k+1} = \mathcal{S}_{\frac{\lambda}{\mu_k}}\Big(\mathcal{P}_\Omega(\mathbf{D}) - \mathbf{X}_{k+1} - \mathbf{S}_k + \mu_k^{-1}\mathbf{\Lambda}_k\Big). \tag{41}$$

Note that all the optimization variables $\mathbf{X}$, $\mathbf{E}$, $\mathbf{S}$, and $\mathbf{\Lambda}$ are updated by closed-form solutions in (38), (41), (39), and (37), respectively, whereas $\mathbf{X}$ is solved iteratively in [8]. Therefore, the proposed algorithm is computationally more efficient than the conventional matrix completion-based approach in [8] as will be shown in Section V-B. Also, note that rank minimization-based HDR imaging may yield artifacts in the presence of large moving objects with small motions. This is because the overlapping parts across input images

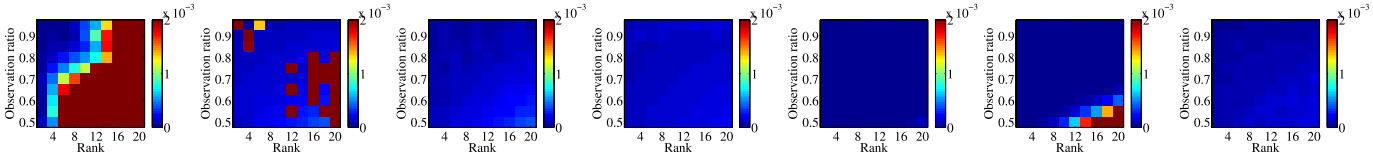

(a) OptSpace (b) LMaFit (c) IALM-MC (d) TNNR-ADMM (e) IRNN-TNN (f) PSSV-MC (g) TNNM-ALM

Fig. 1. Comparison of normalized reconstruction errors for synthetic data with varying rank r_0 and observation ratio $|\Omega|/(mn)$. (a) OptSpace [21], (b) LMaFit [22], (c) IALM-MC [16], (d) TNNR-ADMM [20], (e) IRNN-TNN [24], (f) PSSV-MC [25], and (g) TNNM-ALM. The color magnitude represents the normalized reconstruction error.

would remain in the low-rank matrix while non-overlapping parts would be removed. While global image registration has been incorporated into the rank minimization framework [8], [47], dealing with local motions still remains a significant open challenge.

C. HDR Image Composition

We synthesize an HDR image by averaging the background irradiance maps in the low-rank matrix $\mathbf{X}$, *i.e.*, we compose an HDR image by

$$R_i = \frac{1}{n}\sum_{j=1}^{n} X_{ij}, \tag{42}$$

where R_i is the estimated radiance at pixel location i.

The simple synthesis scheme in (42) may cause artifacts, especially in a region where the moving objects are poorly exposed. More sophisticated algorithms have been developed to handle such regions and provide higher-quality results [36].

V. Experimental Results

We evaluate the performance of the proposed TNNM-ALM algorithm on synthetic data, and then compare our HDR results with those of the state-of-the-art HDR imaging algorithms. We first compare the performance of TNNM-ALM with conventional truncated nuclear norm minimization algorithms, *i.e.*, TNNR [20], the iteratively reweighted nuclear norm (IRNN) algorithm [24], and PSSV for matrix completion (PSSV-MC) [25]. We use ADMM to solve a subproblem of TNNR and define g_i's and their supergradients ∂g_i's of IRNN to minimize the truncated nuclear norm as

$$g_i(x) = \begin{cases} 0, & \text{if } i \le r, \\ x, & \text{otherwise}, \end{cases} \qquad \partial g_i(x) = \begin{cases} 0, & \text{if } i \le r, \\ 1, & \text{otherwise}, \end{cases}$$

which are denoted as TNNR-ADMM and IRNN-TNN, respectively. In addition, we compare TNNM-ALM with the state-of-the-art matrix completion algorithms, *i.e.*, OptSpace [21], low-rank matrix fitting (LMaFit) [22], and IALM-MC [16]. The results of conventional algorithms are obtained by executing the codes provided by the respective authors.

All parameters in the conventional algorithms are fixed to the default values presented in each paper. As noted in [13], for a white noise with standard deviation σ, δ in (7) satisfies $\delta^2 \le \left(|\Omega| + \sqrt{8|\Omega|}\right)\sigma^2$ with high probability, where $|\Omega|$ denotes the number of observations. Following this property, we set $\delta = \left(|\Omega| + \sqrt{8|\Omega|}\right)^{\frac{1}{2}}\sigma$. Also, in all experiments, we set $\mu_1 = \frac{1.25}{\sigma_1(\mathbf{D})}$, $\mu_{\max} = 10^6$, $\rho = 1.5$, and $\kappa = 2 \times 10^{-3}$ in (28). For reproducibility, we also provide our MATLAB implementation on our project website.[1]

A. Synthetic Data

We compare the performance on synthetic data in terms of reconstruction error, execution time, and robustness against noise. We synthesize a ground-truth matrix $\mathbf{X}_0 \in \mathbb{R}^{m\times n}$, composed of two matrices of rank r_0, *i.e.*, $\mathbf{X}_L \in \mathbb{R}^{m\times r_0}$ and $\mathbf{X}_R \in \mathbb{R}^{r_0\times n}$, elements of which are the sum of two variables sampled from the standard normal distribution $\mathcal{N}(0,1)$ and the uniform distribution $\mathcal{U}(-0.5, 0.5)$, respectively, and then set $\mathbf{X}_0 = \mathbf{X}_L\mathbf{X}_R$. The locations of observed indices Ω are uniformly sampled at random. Finally, each element in $\mathbf{X}_0$ is corrupted by an additive noise that has a normal distribution $\mathcal{N}(0, \sigma^2)$. To evaluate the performance of matrix completion, we measure the normalized reconstruction error $\frac{\|\mathbf{X}_0 - \widehat{\mathbf{X}}\|_F}{\|\mathbf{X}_0\|_F}$ between the ground-truth matrix $\mathbf{X}_0$ and recovered matrix $\widehat{\mathbf{X}}$. We fix the matrix size to $m = 1000$ and $n = 100$, but note that the execution time of the proposed algorithm is proportional to the matrix size. The average performance over 30 trials for each set of parameters is reported below.

First, we evaluate the reconstruction performance over various values of both matrix rank r_0 and observation ratio $|\Omega|/(mn)$. In this test, we assume noiseless observations, *i.e.*, $\sigma = 0$. Fig. 1 compares the normalized reconstruction errors of the proposed TNNM-ALM with those of the conventional algorithms. We see that the matrix factorization-based approaches show the worst performance. Specifically, OptSpace yields poor reconstruction performance, and LMaFit fails to converge to global solutions under several settings where it yields high reconstruction errors. Since IALM-MC does not exploit *a priori* rank information, its reconstruction performance gets worse as the rank increases and the observation ratio decreases. The results on PSSV-MC show similar tendencies to those of IALM-MC. These results indicate that their reconstruction performance for complex structures of matrices is not as good as those for simple cases. In contrast, TNNR-ADMM, IRNN-TNN, and TNNM-ALM provide lower reconstruction errors than OptSpace, LMaFit, IALM-MC, and PSSV-MC, achieving better reconstruction of the structure of low-rank matrices.

Fig. 2 compares the average execution times to obtain the results in Fig. 1. We use a PC with a 2.1 GHz CPU and 8 GB RAM. All algorithms are implemented in MATLAB.

[1] http://www.eee.hku.hk/~chullee/research/tnnm_alm.html

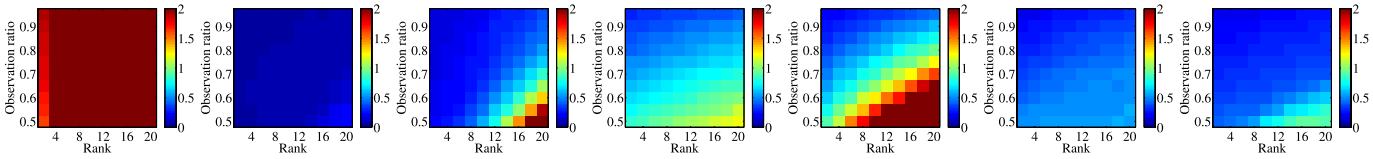

Fig. 2. Comparison of execution times for synthetic data with varying rank r_0 and observation ratio $|\Omega|/(mn)$. (a) OptSpace [21], (b) LMaFit [22], (c) IALM-MC [16], (d) TNNR-ADMM [20], (e) IRNN-TNN [24], (f) PSSV-MC [25], and (g) TNNM-ALM. The color magnitude represents the execution time in seconds.

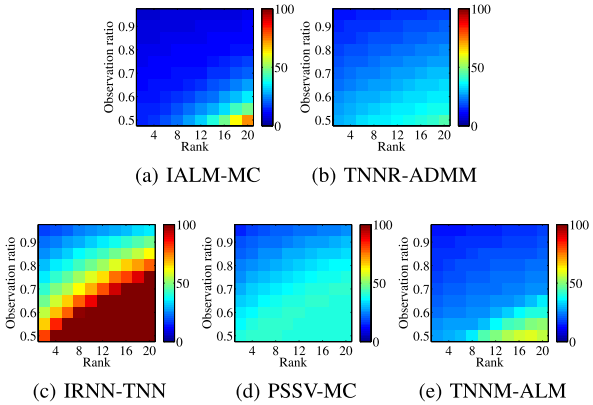

Fig. 3. Comparison of the number of SVD computations for synthetic data with varying rank r_0 and observation ratio $|\Omega|/(mn)$. (a) IALM-MC [16], (b) TNNR-ADMM [20], (c) IRNN-TNN [24], (d) PSSV-MC [25], and (e) TNNM-ALM. The color magnitude represents the number of SVD computations.

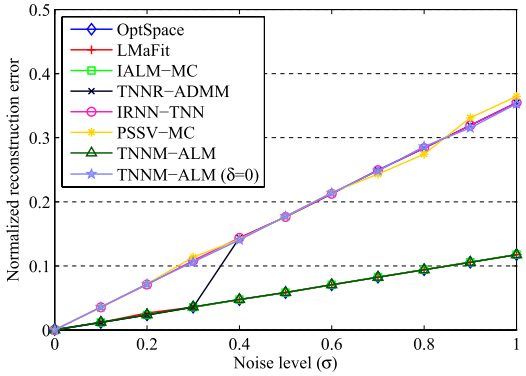

Fig. 4. Comparison of normalized reconstruction errors at different noise levels when the observation ratio is 0.7 and $r_0 = 5$.

We see that OptSpace is the most inefficient and LMaFit is the most efficient in terms of execution time. The execution times of IALM-MC, TNNR-ADMM, and IRNN-TNN get higher as rank increases and observation ratio decreases. On the other hand, the execution times of PSSV-MC and TNNM-ALM are significantly less than those of IALM-MC, TNNR-ADMM and IRNN-TNN to be comparable to LMaFit, achieving matrix completion more efficiently due to variable updates via closed-form solutions at each iteration of the ALM method. Note that the main computational cost of the nuclear norm or truncated nuclear norm minimization-based approaches, *i.e.*, IALM-MC, TNNR-ADMM, IRNN-TNN, PSSV-MC, and TNNM-ALM, lies in computing the SVD for soft-thresholding at each iteration. Therefore, in addition to execution times, we compare the number of SVD computations for these algorithms. Fig. 3 compares the average number of SVD computations to obtain the results in Fig. 1. The results in Fig. 3 exhibit similar tendencies to those in Fig. 2. Note that we only need singular values that are larger than a threshold by the soft-thresholding operator in (24). Therefore, we can achieve further speedup by computing only the first few singular values and their corresponding singular vectors instead of the full SVD as done in [9], [14], and [16] or by employing a fast approximate SVT [49]. For example, in [49], it is shown that the fast approximate SVT can achieve about five-times speedups over the full SVD for a practical application of the TNNM-based RPCA.

The proposed TNNM-ALM considers noise components in observed data, and as discussed earlier, the parameter δ in (7) is determined by the noise level σ. Fig. 4 shows the reconstruction performance for various values of σ, when the observation ratio is 0.7 and $r_0 = 5$. We see that the proposed TNNM-ALM provides significantly lower reconstruction errors than conventional truncated nuclear norm minimization algorithms, *i.e*, TNNR-ADMM, IRNN-TNN, and PSSV-MC, and comparable to OptSpace, LMaFit, and IALM-MC. More specifically, TNNR-ADMM provides comparable reconstruction performances to TNNM-ALM at lower noise levels but yields higher errors as the noise level increases, *i.e.*, at regions with $\sigma \geq 0.4$. Therefore, these results confirm that the proposed TNNM-ALM can estimate missing data more accurately from noisy observations. In addition, Fig. 4 shows that TNNM-ALM yields higher reconstruction errors when the noise parameter δ in (7) is incorrectly set, *i.e.*, $\delta = 0$ for all values of σ. In such a case, TNNM-ALM provides comparable reconstruction performance to IRNN-TNN and PSSV-MC, which can be regarded as the lower bound for TNNM-ALM in terms of accuracy of noise estimation.

Finally, we examine the convergence behavior of TNNM-ALM. Fig. 5 plots the normalized reconstruction error $\frac{\|\mathbf{X}_0 - \mathbf{X}_k\|_F}{\|\mathbf{X}_0\|_F}$ and the stopping criterion in (29) at all iterations. We generate test matrices of rank 5 with different values of observation ratio and σ, *i.e.*, ratio $= 0.5, 0.7$ and $\sigma = 0, 0.5$, respectively, and compute the average values over the trials. In all cases, the normalized reconstruction error monotonically decreases, which reveals the convergence to a stationary point despite the nonconvexity of the problem. In addition, not surprisingly, Fig. 5(a) shows that, as the observation ratio gets higher and as the noise level gets smaller, TNNM-ALM provides higher accuracy.

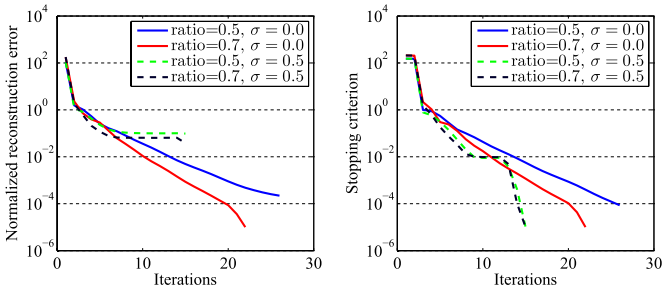

Fig. 5. Convergence behavior of TNNM-ALM. (a) Normalized reconstruction error and (b) stopping criterion.

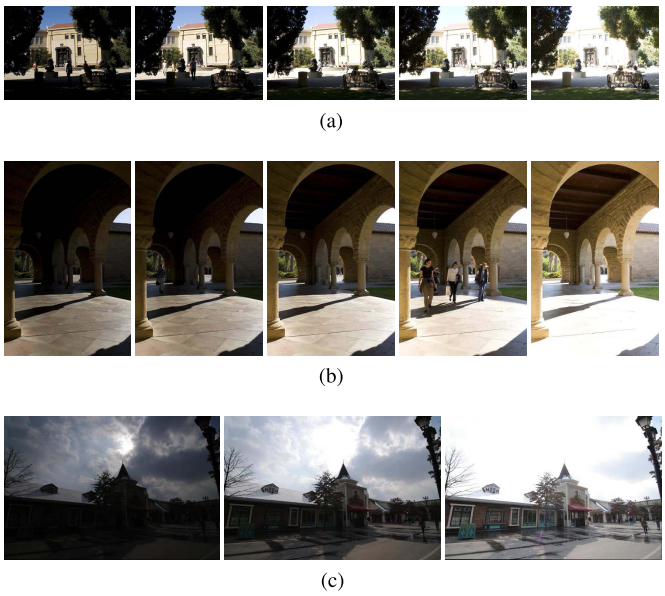

Fig. 6. The input image sets. (a) *SculptureGarden*, (b) *Arch*, and (c) *AmusementPark*. The exposure times of each data set are (1/320, 1/160, 1/80, 1/40, 1/20), (1/500, 1/250, 1/125, 1/60, 1/30), and (1/5000, 1/1250, 1/320) seconds, respectively.

B. Application to Ghost-Free HDR Image Synthesis

We evaluate the performance of the proposed HDR image synthesis algorithm on three image data sets, *i.e.*, the *SculptureGarden* and *Arch* sets [37] with five images and the *AmusementPark* set [26] with three images in Fig. 6. The parameters δ and λ in (32) and (33) are set to 0 and $1/\sqrt{\max(m,n)}$, respectively, unless otherwise specified. We define the observed region as a set of properly-exposed pixel locations, given by

$$\Omega = \{(i,j) | Z_{\text{th}} \leq Z_{ij} \leq 255 - Z_{\text{th}}\}, \tag{43}$$

where the threshold value is fixed to $Z_{\text{th}} = 2$ in this work. Note, however, that the observed region Ω can be chosen using any ghost region detection techniques [34] or even manually by a user [8]. We compare the proposed algorithm with two PSSV-based algorithms: RPCA-based algorithm (PSSV-RPCA) and matrix completion-based algorithm (PSSV-MC) [8], both of which are applications of PSSV [23], [25] to HDR imaging and contain more tools to improve image quality. We use the MATLAB function `tonemap` to display the results of the proposed algorithm, Hu *et al.*'s algorithm [27], Lee *et al.*'s algorithm [7], PSSV-RPCA [8], and PSSV-MC [8], while Heo *et al.*'s algorithm [26] uses their own tone mapping technique. Due to the different tone mapping, we compare only the amount of details and artifacts in the tone-mapped images qualitatively, instead of comparing differences of colors and brightness. Also, since no object metric to quantitatively evaluate the performance of the ghost-free HDR imaging algorithms has been developed [34], we provide only the subjective assessment. The results of the conventional algorithms are obtained by executing the codes provided by the respective authors.

Fig. 7 compares the synthesized results and their detailed parts on the *SculptureGarden* images. In Figs. 7(a)–(c), Heo *et al.*'s, Hu *et al.*'s, and Lee *et al.*'s algorithms provide HDR images with moving objects from one of the input images, whereas PSSV-RPCA, PSSV-MC, and the proposed algorithm yield the background scene in Figs. 7(d)–(f). This is because we define Ω as a set of properly-exposed pixels only, but note that we can also produce output HDR images that contain objects in an input image by employing ghost region detection [34]. In Fig. 7(a), Heo *et al.*'s algorithm provides results with severe artifacts, *e.g.*, smeared textures on the ground and color distortions on the stairs, due to incorrect ghost region detection. Hu *et al.*'s algorithm in Fig. 7(b) provides images without ghosting artifacts but yields blurring artifacts near the boundaries of walking people, where correspondence matching fails due to poor exposure in the reference image. Lee *et al.*'s algorithm in Fig. 7(c) preserves image details and removes ghosting artifacts effectively, but still provides color artifacts in highly saturated regions. PSSV-RPCA in Fig. 7(d) yields severe ghosting artifacts and loses textures in saturated regions. Finally, PSSV-MC and the proposed algorithm in Figs. 7(e) and (f), respectively, produce comparable results, effectively removing ghosting artifacts, but the proposed algorithm requires significantly lower computational resources as will be shown later. Note, however, that the results of PSSV-MC and the proposed algorithm still have artifacts in a region where the moving objects and background are poorly exposed.

Fig. 8 further shows the synthesized HDR images and their magnified parts on the *Arch* images, obtained by each algorithm. Although all algorithms effectively remove ghosting artifacts, Heo *et al.*'s algorithm loses textures in the ceiling in Fig. 8(a). Hu *et al.*'s algorithm provides blurring artifacts in the ceiling in Fig. 8(b), because of the failure of the correspondence estimation at poorly-exposed regions. PSSV-RPCA in Fig. 8(d) provides ghosting artifacts. As we may observe, Lee *et al.*'s algorithm, PSSV-MC, and the proposed algorithm yield comparable results that remove ghosting artifacts effectively while preserving image details.

We also evaluate the performance of different algorithms when the input images are corrupted by noise. Additive zero-mean white Gaussian noise components with noise level $\sigma = 20$ are added to input images in the experiments. Note, however, that the noise level can also be estimated from noisy input images [50], [51]. Fig. 9 compares the detailed parts of

(a) (b) (c) (d) (e) (f)

Fig. 7. Synthesized results of the *SculptureGarden* image set by (a) Heo *et al.*'s algorithm [26], (b) Hu *et al.*'s algorithm [27], (c) Lee *et al.*'s algorithm [7], (d) PSSV-RPCA [8], (e) PSSV-MC [8], and (f) the proposed algorithm.

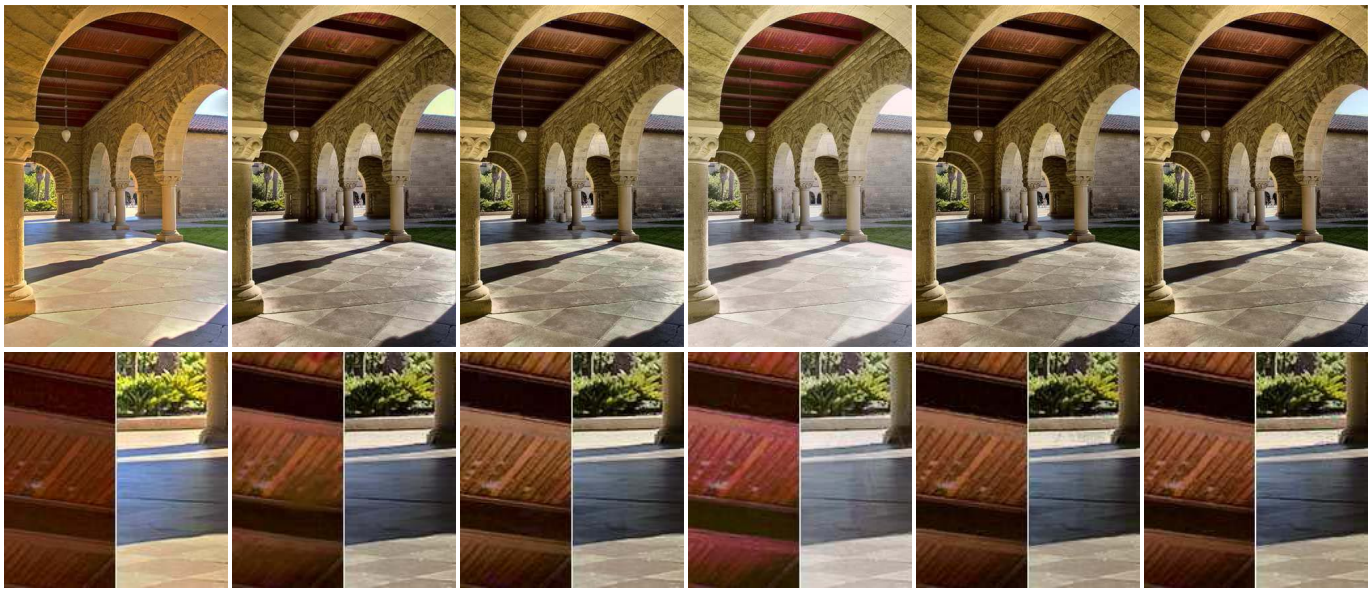

(a) (b) (c) (d) (e) (f)

Fig. 8. Synthesized results of the *Arch* image set by (a) Heo *et al.*'s algorithm [26], (b) Hu *et al.*'s algorithm [27], (c) Lee *et al.*'s algorithm [7], (d) PSSV-RPCA [8], (e) PSSV-MC [8], and (f) the proposed algorithm.

(a) (b) (c) (d) (e) (f)

Fig. 9. Synthesized results of the *AmusementPark* image set at $\sigma = 20$. The images are synthesized by (a) Heo *et al.*'s algorithm [26], (b) Hu *et al.*'s algorithm [27], (c) Lee *et al.*'s algorithm [7], (d) PSSV-RPCA [8], (e) PSSV-MC [8], and (f) the proposed algorithm.

the synthesized results on the *AmusementPark* images. The results of all the conventional algorithms in Figs. 9(a)–(e) contain noise components from noisy input images, *e.g.*, on the signboard and the facade of the building. On the contrary, the proposed algorithm in Fig. 9(f) removes noise components effectively, providing the highest image quality, since we take into account the noise level in the input images in the formulation in (32).

Table I compares the actual execution times for the *SculptureGarden* and *Arch* sets with five images of resolution 1024×754 and 669×1024, respectively. PSSV-RPCA is the most efficient in terms of execution time, but, as shown

TABLE I

THE COMPUTATION TIMES IN SECONDS OF Heo *et al.*'s ALGORITHM [26], Hu *et al.*'s ALGORITHM [27], Lee *et al.*'s ALGORITHM [7], PSSV-RPCA [8], PSSV-MC [8], AND THE PROPOSED ALGORITHM FOR TWO TEST SETS

	Heo *et al.* [26]	Hu *et al.* [27]	Lee *et al.* [7]	PSSV-RPCA [8]	PSSV-MC [8]	Proposed
SculptureGarden	390	392	91	40	149	52
Arch	303	232	154	37	200	51

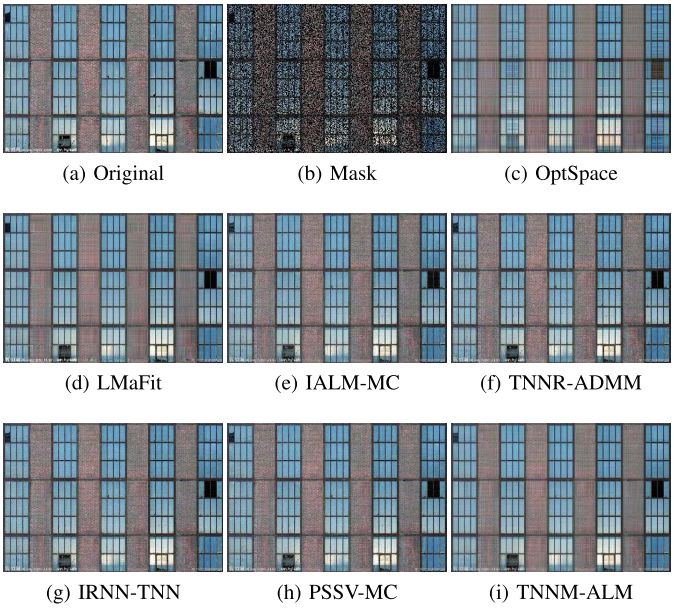

(a) Original (b) Mask (c) OptSpace

(d) LMaFit (e) IALM-MC (f) TNNR-ADMM

(g) IRNN-TNN (h) PSSV-MC (i) TNNM-ALM

Fig. 10. Comparison of recovered images with a random mask of a natural image using different methods when 50% of pixels are observed. (a) Original image [20] and (b) image with mask. Recovered images by (c) OptSpace [21] (21.62 dB), (d) LMaFit [22] (24.71 dB), (e) IALM-MC [16] (25.48 dB), (f) TNNR-ADMM [20] (25.30 dB), (g) IRNN-TNN [33] (25.40 dB), (h) PSSV-MC [25] (25.47 dB), and (i) TNNM-ALM (26.08 dB).

before, it fails to remove ghosting artifacts effectively. Except for PSSV-RPCA, the proposed algorithm is the most efficient, especially compared with PSSV-MC, which is also based on the low-rank matrix completion framework. This is because the proposed algorithm updates the optimization variables by closed-form solutions, whereas PSSV-MC performs it iteratively. These results indicate that the proposed algorithm provides comparable or even better performance than conventional algorithms, while demanding significantly lower computational resources.

C. Application to Image Recovery

In addition to HDR imaging, the proposed TNNM-ALM is applicable to a wide range of imaging applications, which can be formulated as low-rank matrix completion. As an example, as done in [20], we apply the proposed TNNM-ALM to recover natural images when data are randomly observed, based on the assumption that the images can be regarded as approximately low-rank matrices. We recover images with three color channels by applying matrix completion to each channel independently. In this test, we set σ to 10. We test with values of rank in the range $[2, 10]$, then choose the best result as the recovered image.

Fig. 10 compares the reconstructed results on the test image when data are randomly observed and shows that the proposed TNNM-ALM provides higher image quality than conventional algorithms. For example, the results of the conventional algorithms contain noise components, while TNNM-ALM removes noise by modeling it explicitly in the formulation. Moreover, TNNM-ALM achieves higher objective qualities. Specifically, the PSNR values of the reconstructed images in Fig. 10 of OptSpace, LMaFit, IALM-MC, TNNR-ADMM, IRNN-TNN, PSSV-MC, and TNNM-ALM are 21.62, 24.71, 25.48, 25.30, 25.40, 25.47, and 26.08 dB, respectively. We also report the actual execution times of all algorithms to obtain the results in Fig. 10 for comparison. OptSpace, LMaFit, IALM-MC, TNNR-ADMM, IRNN-TNN, PSSV-MC, and TNNM-ALM take 13.01, 0.27, 2.43, 30.78, 30.03, 4.71, and 2.77 seconds, respectively. These results confirm that TNNM-ALM can achieve substantial increases in speed over OptSpace, TNNR-ADMM, IRNN-TNN, and PSSV-MC and is comparable to IALM-MC, while providing significantly higher image qualities than all the conventional algorithms.

VI. CONCLUSIONS

We developed a computationally efficient truncated nuclear norm minimization algorithm for matrix completion, called TNNM-ALM. We reformulated the truncated nuclear norm minimization so that an efficient ALM method can be employed in the optimization. Furthermore, we developed an updating scheme of the optimization variables via closed-form solutions at each iteration during the optimization. We then extended the proposed TNNM-ALM to ghost-free HDR image synthesis. Experimental results on both synthetic and real visual datasets showed that TNNM-ALM can provide comparable or even higher reconstruction performance than conventional truncated nuclear norm minimization algorithms, while achieving substantial increases in speed. Since the truncated nuclear norm can achieve a better approximation of the matrix rank than the nuclear norm and the proposed TNNM-ALM can minimize the truncated nuclear norm efficiently, we expect that TNNM-ALM could be further extended for various imaging applications. Some of the important directions for future work are to analyze theoretical convergence properties of TNNM-ALM, to incorporate local object motions [52] into the rank minimization framework for HDR imaging, and to develop objective metrics for ghost-free HDR imaging.

REFERENCES

[1] E. J. Candès and B. Recht, "Exact matrix completion via convex optimization," *Found. Comput. Math.*, vol. 9, no. 6, pp. 717–772, Dec. 2009.

[2] X. Zhou, C. Yang, and W. Yu, "Moving object detection by detecting contiguous outliers in the low-rank representation," *IEEE Trans. Pattern Anal. Mach. Intell.*, vol. 35, no. 3, pp. 597–610, Mar. 2013.

[3] H. Ji, C. Liu, Z. Shen, and Y. Xu, "Robust video denoising using low rank matrix completion," in *Proc. IEEE Conf. Comput. Vis. Pattern Recognit.*, Jun. 2010, pp. 1791–1798.

[4] R. Cabral, F. De la Torre, J. P. Costeira, and A. Bernardino, "Matrix completion for weakly-supervised multi-label image classification," *IEEE Trans. Pattern Anal. Mach. Intell.*, vol. 37, no. 1, pp. 121–135, Jan. 2015.

[5] Y. Luo, T. Liu, D. Tao, and C. Xu, "Multiview matrix completion for multilabel image classification," *IEEE Trans. Image Process.*, vol. 24, no. 8, pp. 2355–2368, Aug. 2015.

[6] G. Tsagkatakis and P. Tsakalides, "Efficient high dynamic range imaging via matrix completion," in *Proc. IEEE Int. Workshop Mach. Learn. Signal Process.*, Sep. 2012, pp. 1–6.

[7] C. Lee, Y. Li, and V. Monga, "Ghost-free high dynamic range imaging via rank minimization," *IEEE Signal Process. Lett.*, vol. 21, no. 9, pp. 1045–1049, Sep. 2014.

[8] T. H. Oh, J. Y. Lee, Y. W. Tai, and I. S. Kweon, "Robust high dynamic range imaging by rank minimization," *IEEE Trans. Pattern Anal. Mach. Intell.*, vol. 37, no. 6, pp. 1219–1232, Jun. 2015.

[9] J.-F. Cai, E. J. Candès, Z. Shen, "A singular value thresholding algorithm for matrix completion," *SIAM J. Optim.*, vol. 20, no. 4, pp. 1956–1982, 2010.

[10] B. Recht, M. Fazel, and P. A. Parrilo, "Guaranteed minimum-rank solutions of linear matrix equations via nuclear norm minimization," *SIAM Rev.*, vol. 52, no. 3, pp. 471–501, 2010.

[11] S. Ma, D. Goldfarb, and L. Chen, "Fixed point and Bregman iterative methods for matrix rank minimization," *Math. Program.*, vol. 128, nos. 1–2, pp. 321–353, 2011.

[12] E. J. Candès and T. Tao, "The power of convex relaxation: Near-optimal matrix completion," *IEEE Trans. Inf. Theory*, vol. 56, no. 5, pp. 2053–2080, May 2010.

[13] E. J. Candès and Y. Plan, "Matrix completion with noise," *Proc. IEEE*, vol. 98, no. 6, pp. 925–936, Jun. 2010.

[14] K.-C. Toh and S. Yun, "An accelerated proximal gradient algorithm for nuclear norm regularized linear least squares problems," *Pacific J. Optim.*, vol. 6, no. 3, pp. 615–640, Nov. 2010.

[15] R. Mazumder, T. Hastie, and R. Tibshirani, "Spectral regularization algorithms for learning large incomplete matrices," *J. Mach. Learn. Res.*, vol. 11, pp. 2287–2322, Jan. 2010.

[16] Z. Lin, M. Chen, L. Wu, and Y. Ma, "The augmented Lagrange multiplier method for exact recovery of corrupted low-rank matrices," Dept. Electr. Comput. Eng., Univ. Illinois Urbana–Champaign, Champaign, IL, USA, Tech. Rep. UILU-ENG-09-2215, Nov. 2009.

[17] J. Wright, A. Ganesh, S. Rao, Y. Peng, and Y. Ma, "Robust principal component analysis: Exact recovery of corrupted low-rank matrices by convex optimization," in *Proc. Adv. Neural Inf. Process. Syst.*, Dec. 2009, pp. 2080–2088.

[18] H. Hayakawa, "Photometric stereo under a light source with arbitrary motion," *J. Opt. Soc. Amer. A*, vol. 11, no. 11, pp. 3079–3089, Nov. 1994.

[19] L. Wu, A. Ganeshy, B. Shi, Y. Matsushita, Y. Wang, and Y. Ma, "Robust photometric stereo via low-rank matrix completion and recovery," in *Proc. Asian Conf. Comput. Vis.*, Nov. 2010, pp. 703–717.

[20] Y. Hu, D. Zhang, J. Ye, X. Li, and X. He, "Fast and accurate matrix completion via truncated nuclear norm regularization," *IEEE Trans. Pattern Anal. Mach. Intell.*, vol. 35, no. 9, pp. 2117–2130, Sep. 2013.

[21] R. H. Keshavan, A. Montanari, and S. Oh, "Matrix completion from a few entries," *IEEE Trans. Inf. Theory*, vol. 56, no. 6, pp. 2980–2998, Jun. 2010.

[22] Z. Wen, W. Yin, and Y. Zhang, "Solving a low-rank factorization model for matrix completion by a nonlinear successive over-relaxation algorithm," *Math. Program. Comput.*, vol. 4, no. 4, pp. 333–361, Dec. 2012.

[23] T.-H. Oh, H. Kim, Y.-W. Tai, J.-C. Bazin, and I. S. Kweon, "Partial sum minimization of singular values in RPCA for low-level vision," in *Proc. IEEE Int. Conf. Comput. Vis.*, Dec. 2013, pp. 145–152.

[24] C. Lu, J. Tang, S. Yan, and Z. Lin, "Generalized nonconvex nonsmooth low-rank minimization," in *Proc. IEEE Conf. Comput. Vis. Pattern Recognit.*, Jun. 2014, pp. 4130–4137.

[25] T.-H. Oh, Y.-W. Tai, J.-C. Bazin, H. Kim, and I. S. Kweon, "Partial sum minimization of singular values in robust PCA: Algorithm and applications," *IEEE Trans. Pattern Anal. Mach. Intell.*, vol. 38, no. 4, pp. 744–758, Apr. 2016.

[26] Y. S. Heo, K. M. Lee, S. U. Lee, Y. Moon, and J. Cha, "Ghost-free high dynamic range imaging," in *Proc. Asian Conf. Comput. Vis.*, Nov. 2010, pp. 486–500.

[27] J. Hu, O. Gallo, K. Pulli, and X. Sun, "HDR deghosting: How to deal with saturation?" in *Proc. IEEE Conf. Comput. Vis. Pattern Recognit.*, Jun. 2013, pp. 1163–1170.

[28] M. Fazel, "Matrix rank minimization with applications," Ph.D. dissertation, Dept. Electr. Eng., Stanford Univ., Stanford, CA, USA, Mar. 2002.

[29] S. Ji and J. Ye, "An accelerated gradient method for trace norm minimization," in *Proc. Annu. Int. Conf. Mach. Learn.*, Jun. 2009, pp. 457–464.

[30] A. Eriksson and A. van den Hengel, "Efficient computation of robust weighted low-rank matrix approximations using the L_1 norm," *IEEE Trans. Pattern Anal. Mach. Intell.*, vol. 34, no. 9, pp. 1681–1690, Sep. 2012.

[31] E. J. Candès, X. Li, Y. Ma, and J. Wright, "Robust principal component analysis?" *J. ACM*, vol. 58, no. 3, p. 11, May 2011.

[32] K. Chen, H. Dong, and K.-S. Chan, "Reduced rank regression via adaptive nuclear norm penalization," *Biometrika*, vol. 100, no. 4, pp. 901–920, Sep. 2013.

[33] S. Gu, L. Zhang, W. Zuo, and X. Feng, "Weighted nuclear norm minimization with application to image denoising," in *Proc. IEEE Int. Conf. Comput. Vis. Pattern Recognit.*, Jun. 2014, pp. 2862–2869.

[34] O. T. Tursun, A. O. Akyüz, A. Erdem, and E. Erdem, "The state of the art in HDR deghosting: A survey and evaluation," *Comput. Graph. Forum*, vol. 34, no. 2, pp. 683–707, May 2015.

[35] P. Sen, N. K. Kalantari, M. Yaesoubi, S. Darabi, D. B. Goldman, and E. Shechtman, "Robust patch-based HDR reconstruction of dynamic scenes," *ACM Trans. Graph.*, vol. 31, no. 6, Nov. 2012, Art. no. 203.

[36] J. Zheng, Z. Li, Z. Zhu, S. Wu, and S. Rahardja, "Hybrid patching for a sequence of differently exposed images with moving objects," *IEEE Trans. Image Process.*, vol. 22, no. 12, pp. 5190–5201, Dec. 2013.

[37] O. Gallo, N. Gelfand, W.-C. Chen, M. Tico, and K. Pulli, "Artifact-free high dynamic range imaging," in *Proc. IEEE Int.Conf. Comput. Photogr.*, Apr. 2009, pp. 1–7.

[38] A. Bhardwaj and S. Raman, "Robust PCA-based solution to image composition using augmented Lagrange multiplier (ALM)," *Vis. Comput.*, vol. 32, no. 5, pp. 591–600, May 2016.

[39] M. Tao and X. Yuan, "Recovering low-rank and sparse components of matrices from incomplete and noisy observations," *SIAM J. Optim.*, vol. 21, no. 2, pp. 57–81, 2011.

[40] E. T. Hale, W. Yin, and Y. Zhang, "Fixed-point continuation for ℓ_1-minimization: Methodology and convergence," *SIAM J. Optim.*, vol. 19, no. 3, pp. 1107–1130, 2008.

[41] S. Boyd and L. Vandenberghe, *Convex Optimization*. Cambridge, U.K.: Cambridge Univ. Press, 2004.

[42] A. Ganesh, Z. Lin, J. Wright, L. Wu, M. Chen, and Y. Ma, "Fast algorithms for recovering a corrupted low-rank matrix," in *Proc. Comput. Adv. Multi-Sens. Adaptive Process.*, Dec. 2009, pp. 213–216.

[43] M. J. D. Powell, "A method for nonlinear constraints in minimization problems," in *Optimization*, R. Fletcher, Ed. New York, NY, USA: Academic, 1969, pp. 283–298.

[44] J. Nocedal and S. J. Wright, *Numerical Optimization*, 2nd ed. New York, NY, USA: Springer, 2006.

[45] S. Boyd, N. Parikh, E. Chu, B. Peleato, and J. Eckstein, "Distributed optimization and statistical learning via the alternating direction method of multipliers," *Found. Trends Mach. Learn.*, vol. 3, no. 1, pp. 1–122, Jan. 2011.

[46] Z. Lin, R. Liu, and Z. Su, "Linearized alternating direction method with adaptive penalty for low-rank representation," in *Proc. Adv. Neural Inf. Process. Syst.*, Dec. 2011, pp. 612–620.

[47] Y. Peng, A. Ganesh, J. Wright, W. Xu, and Y. Ma, "RASL: Robust alignment by sparse and low-rank decomposition for linearly correlated images," *IEEE Trans. Pattern Anal. Mach. Intell.*, vol. 34, no. 11, pp. 2233–2246, Nov. 2012.

[48] J.-Y. Lee, Y. Matsushita, B. Shi, I. S. Kweon, and K. Ikeuchi, "Radiometric calibration by rank minimization," *IEEE Trans. Pattern Anal. Mach. Intell.*, vol. 35, no. 1, pp. 144–156, Jan. 2013.

[49] T.-H. Oh, Y. Matsushita, Y.-W. Tai, and I. S. Kweon, "Fast randomized singular value thresholding for nuclear norm minimization," in *Proc. IEEE Conf. Comput. Vis. Pattern Recognit.*, Jun. 2015, pp. 4484–4493.

[50] G. E. Healey and R. Kondepudy, "Radiometric CCD camera calibration and noise estimation," *IEEE Trans. Pattern Anal. Mach. Intell.*, vol. 16, no. 3, pp. 267–276, Mar. 1994.

[51] C. Liu, R. Szeliski, S. B. Kang, C. L. Zitnick, and W. T. Freeman, "Automatic estimation and removal of noise from a single image," *IEEE Trans. Pattern Anal. Mach. Intell.*, vol. 30, no. 2, pp. 299–314, Feb. 2008.

[52] O. Gallo, A. Troccoli, J. Hu, K. Pulli, and J. Kautz, "Locally non-rigid registration for mobile HDR photography," in *Proc. IEEE Conf. Comput. Vis. Pattern Recognit. Workshops*, Jun. 2015, pp. 48–55.

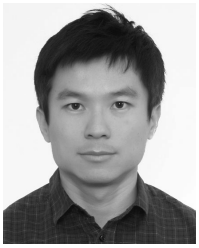

Chul Lee (S'06–M'13) received the B.S., M.S., and Ph.D. degrees from Korea University, Seoul, South Korea, in 2003, 2008, and 2013, respectively, all in electrical engineering.

He was with Biospace Inc., Seoul, South Korea, from 2002 to 2006, where he was involved in the development of medical equipment. From 2013 to 2014, he was a Post-Doctoral Scholar with the Department of Electrical Engineering, Pennsylvania State University, University Park, PA, USA. From 2014 to 2015, he was a Research Scientist with the Department of Electrical and Electronic Engineering, The University of Hong Kong, Hong Kong. In 2015, he joined the Department of Computer Engineering, Pukyong National University, Busan, South Korea, where he is currently an Assistant Professor. His current research interests include image restoration, power-constrained contrast enhancement, and high dynamic range imaging.

Dr. Lee received the best paper award from the *Journal of Visual Communication and Image Representation* in 2014.

Edmund Y. Lam (M'00–SM'05–F'15) received the B.S., M.S., and Ph.D. degrees from Stanford University, Stanford, CA, USA, all in electrical engineering. He conducted research for the programmable digital camera project with the Information Systems Laboratory, Stanford University. He also consulted for industry in the areas of digital camera systems design and algorithms development.

He is currently a Professor in electrical and electronic engineering with The University of Hong Kong (HKU), and serves as the Computer Engineering Program Director. His main research is in computational imaging, and he heads the Photonics and Imaging Technology Cluster with HKU (PITCH). He is a fellow of the Optical Society, the Society of Photo-Optical Instrumentation Engineers, and Hong Kong Institution of Engineers. He is a recipient of the IBM Faculty Award. From 2010 to 2011, he was invited to teach with the Department of Electrical Engineering and Computer Science, Massachusetts Institute of Technology, as a Visiting Associate Professor.

He is currently an Associate Editor of the IEEE TRANSACTIONS ON BIOMEDICAL CIRCUITS AND SYSTEMS and the IEEE SIGNAL PROCESSING LETTERS.